Solving inverse problems for optical scanning holography using an adaptively iterative shrinkage-thresholding algorithm

Fengjun Zhao,[1,5] Xiaochao Qu,[1,5] Xin Zhang,[2] Ting-Chung Poon,[3] Taegeun Kim[4], You Seok Kim[4], and Jimin Liang[1,*]

[1]*School of Life Sciences and Technology, Xidian University, Xi'an, Shaanxi 710126, China*
[2]*Center for Computational Medicine, National Laboratory of Pattern Recognition, Institute of Automation, Chinese Academy of Sciences, Beijing, 100190, China*
[3]*Bradley Department of Electrical and Computer Engineering, Virginia Tech, Blacksburg, Virginia 24061, USA*
[4]*Department of Optical Engineering, Sejong University, 98 Kunja-dong, Kwangjin-gu, Seoul 134-747, Korea*
[5] Contributed equally to this work
[*] *jimleung@mail.xidian.edu.cn*

Abstract: Optical scanning holography (OSH) records a three-dimensional object into a two-dimensional hologram through two-dimensional optical scanning. The recovery of sectional images from the hologram, termed as an inverse problem, has been previously implemented by conventional methods as well as the use of l_2 norm. However, conventional methods require time consuming processing of section by section without eliminating the defocus noise and the l_2 norm method often suffers from the drawback of over-smoothing. Moreover, these methods require the whole hologram data (real and imaginary parts) to eliminate the twin image noise, whose computation complexity and the sophisticated post-processing are far from desirable. To handle these difficulties, an adaptively iterative shrinkage-thresholding (AIST) algorithm, characterized by fast computation and adaptive iteration, is proposed in this paper. Using only a half hologram data, the proposed method obtained satisfied on-axis reconstruction free of twin image noise. The experiments of multi-planar reconstruction and improvement of depth of focus further validate the feasibility and flexibility of our proposed AIST algorithm.

OCIS codes: (090.1995) Digital holography; (100.3020) Image reconstruction-restoration; (100.3190) Inverse problems; (180.6900) Three-dimensional microscopy.

References and links

1. T.-C. Poon, "Scanning holography and two-dimensional image processing by acousto-optic two-pupil synthesis," J. Opt. Soc. Am. A **2**(4), 521–527 (1985).
2. B. D. Duncan and T.-C. Poon, "Gaussian beam analysis of optical scanning holography," J. Opt. Soc. Am. A **9**(2), 229–236 (1992).
3. J. Swoger, M. Martínez-Corral, J. Huisken, and E. H. Stelzer, "Optical scanning holography as a technique for high-resolution three-dimensional biological microscopy," J. Opt. Soc. Am. A **19**(9), 1910–1918 (2002).
4. E. Y. Lam, X. Zhang, H. Vo, T.-C. Poon, and G. Indebetouw, "Three-dimensional microscopy and sectional image reconstruction using optical scanning holography," Appl. Opt. **48**(34), H113–H119 (2009).
5. G. Indebetouw and W. Zhong, "Scanning holographic microscopy of three-dimensional fluorescent specimens," J. Opt. Soc. Am. A **23**(7), 1699–1707 (2006).
6. G. Indebetouw, A. El Maghnouji, and R. Foster, "Scanning holographic microscopy with transverse resolution exceeding the Rayleigh limit and extended depth of focus," J. Opt. Soc. Am. A **22**(5), 892–898 (2005).
7. T. Kim, "Optical sectioning by optical scanning holography and a Wiener filter," Appl. Opt. **45**(5), 872–879 (2006).
8. H. Kim, S.-W. Min, B. Lee, and T.-C. Poon, "Optical sectioning for optical scanning holography using phase-space filtering with Wigner distribution functions," Appl. Opt. **47**(19), D164–D175 (2008).
9. X. Zhang, E. Y. Lam, and T.-C. Poon, "Reconstruction of sectional images in holography using inverse imaging," Opt. Express **16**(22), 17215–17226 (2008).

#160246 - $15.00 USD Received 19 Dec 2011; revised 14 Feb 2012; accepted 20 Feb 2012; published 27 Feb 2012

10. X. Zhang, E. Y. Lam, T. Kim, Y. S. Kim, and T.-C. Poon, "Blind sectional image reconstruction for optical scanning holography," Opt. Lett. **34**(20), 3098–3100 (2009).
11. S.-J. Kim, K. Koh, M. Lustig, S. Boyd, and D. Gorinevsky, "An interior-point method for large-scale l1-regularizedleast squares," IEEE J. Sel. Top. Signal Process. **1**(4), 606–617 (2007).
12. X. Zhang and E. Y. Lam, "Edge-preserving sectional image reconstruction in optical scanning holography," J. Opt. Soc. Am. A **27**(7), 1630–1637 (2010).
13. S. Wei and H. Xu, "Staircasing reduction model applied to total variation based image reconstruction,"in *17th European Signal Processing Conference* (EUSIPCO, Glasgow, Scotland, 2009), pp. 2579–2583.
14. I. F. Gorodnitsky and B. D. Rao, "Sparse signal reconstruction from limited data using focuss: a re-weighted minimum norm algorithm," IEEE Trans. Signal Process. **45**(3), 600–616 (1997).
15. Y. Lu, X. Zhang, A. Douraghy, D. Stout, J. Tian, T. F. Chan, and A. F. Chatziioannou, "Source reconstruction for spectrally-resolved bioluminescence tomography with sparse a priori information," Opt. Express **17**(10), 8062–8080 (2009).
16. Q. Zhang, H. Zhao, D. Chen, X. Qu, X. Chen, X. He, W. Li, Z. Hu, J. Liu, J. Liang, and J. Tian, "Source sparsity based primal-dual interior-point method for three-dimensional bioluminescence tomography," Opt. Commun. **284**(24), 5871–5876 (2011).
17. X. He, J. Liang, X. Wang, J. Yu, X. Qu, X. Wang, Y. Hou, D. Chen, F. Liu, and J. Tian, "Sparse reconstruction for quantitative bioluminescence tomography based on the incomplete variables truncated conjugate gradient method," Opt. Express **18**(24), 24825–24841 (2010).
18. D. Han, J. Tian, S. Zhu, J. Feng, C. Qin, B. Zhang, and X. Yang, "A fast reconstruction algorithm for fluorescence molecular tomography with sparsity regularization," Opt. Express **18**(8), 8630–8646 (2010).
19. T.-C. Poon, *Optical Scanning Holography with MATLAB* (Springer, New York, 2007).
20. X. Zhang, E. Y. Lam, and T.-C. Poon, "Fast iterative sectional image reconstruction in optical scanning holography," in *Digital Holography and Three-Dimensional Imaging*, Technical Digest (CD) (Optical Society of America, 2009), paper DMA3.
21. S. Chen, D. Donoho, and M. Saunders, "Atomic decomposition by basis pursuit," SIAM Rev. **43**(1), 129–159 (2001).
22. E. Candès, J. Romberg, and T. Tao, "Stable signal recovery from incomplete and inaccurate measurements," Commun. Pure Appl. Math. **59**(8), 1207–1223 (2006).
23. A. Yang, A. Ganesh, S. Sastry, and Y. Ma, "Fast L1-minimization algorithms and an application in robust face recognition: a review," in *proceedings of IEEE International Conference on Image Processing,* (Institute of Electrical and Electronics Engineers, California, 2010), pp. 1849–1852.
24. S. J. Wright, R. D. Nowak, and M. A. Figueiredo, "Sparse Reconstruction by Separable Approximation," IEEET, Signal Process. **57**, 2479–2493 (2009).
25. I. Daubechies, M. Defrise, and C. De Mol, "An iterative thresholding algorithm for linear inverse problems with a sparsity constraint," Commun. Pure Appl. Math. **57**(11), 1413–1457 (2004).
26. P. Combettes and V. Wajs, "Signal recovery by proximal forward backward splitting," Multiscale Model. Simul. **4**(4), 1168–1200 (2005).
27. E. Hale, W. Yin, and Y. Zhang, "A fixed-point continuation method for L1-regularized minimization with applications to compressed sensing," *Tech. Rep. TR07–07* (Rice Univ., Houston, TX, 2007).
28. Z. Wang and A. C. Bovik, "A universal image quality index," IEEE Signal Process. Lett. **9**(3), 81–84 (2002).

1. Introduction

As an unconventional digital holographic technique utilizing an acquired two-dimensional (2D) hologram of an object, optical scanning holography (OSH) can record three-dimensional (3D) information of an object [1, 2]. Especially the capability of recording in an incoherent mode expands its application to 3D optical microscopy [3, 4]. For obtaining an acceptable axial resolution of thick specimens, traditional optical microscopy requires axial scanning. Both confocal microscopy and optical coherent tomography (OCT) can provide high axial resolution and optical sectioned images, but they suffer from the same drawback of a time-consuming axial and lateral scanning process. Unlike these optical microcopies, 3D microscopy using OSH can take the holographic information of biological specimens in three dimensions without axial scanning, and high lateral resolution within 1 μm has been made possible in a scanning holographic fluorescence microscope [5]. Its potential advantages of high image acquisition rates and the abundant information of the reconstructed images offer rapid efficient approach to obtain high-resolution 3D sectional mages for biomedical applications [6].

In order to achieve a good recovery performance of the original 3D object from a measured 2D hologram, sectional image reconstruction is the most important part for OSH. In a conventional method, reconstructing the original sectional image through Fresnel diffraction, was first employed to reconstruct the sectional image of OSH. Based on the conventional method, Wiener filtering [7] and Wigner filtering [8] were applied in OSH

#160246 - $15.00 USD Received 19 Dec 2011; revised 14 Feb 2012; accepted 20 Feb 2012; published 27 Feb 2012

reconstruction and obtained an improved signal-to-noise ratio. Nevertheless, the computation of the spectrum for Wiener filtering relies on the assumption that random noise does not exist, which probably leads to significant errors in practice. Wigner filtering is only feasible for synthetic two-section object under the ideal conditions. The computation complexity and cross-term problem limit its applications.

Aiming at overcoming the drawbacks of these conventional-based methods (Fresnel diffraction, Wiener filtering and Wigner filtering), optimization methods have been applied to reconstruct sectional image of OSH. In optimization, one converts sectional image reconstruction to resolving system of equations, whose inputs are the measured hologram and the system's point spread function, the outputs are sectional images.

The l_2 norm method [9, 10] has been able to reconstruct all the sectional images (not only two sectional images) simultaneously and suppress the defocus noise. However, the l_2 norm-based methods often suffers from the drawback of over-smoothing, such that the localized information is lost during the reconstruction [11]. Employing total variation regularization (TV) and edge preserving reconstruction method has improved the reconstruction performance further [12]. However, the performance of the TV-based method is inevitably attacked by the staircase effect [13].

Some other optimization methods, such as l_1 norm and l_p norm methods (where p is between 0 and 1), have been proposed [14]. By virtue of their excellent ability of noise suppression and accurate reconstruction, these methods have given important value to bioluminescence tomography [15–17] and fluorescence molecular tomography [18]. In this paper, an adaptively iterative shrinkage-thresholding (AIST) algorithm utilizing l_1 norm regularization, which is characterized by fast computation and adaptive iteration, is proposed to study the OSH reconstruction problem.

To avoid the influence of twin image noise, all the previous methods require two parts in OSH physical system, the real part (sine hologram) and the imaginary part (cosine hologram) of the complex hologram [19], which virtually increases the OSH physical system cost and the computational complexity. If it is possible to recover sectional images without twin image noise only using a half hologram data (e.g., the real component or the imaginary component of a complex hologram), it will be invaluable to reduce the system cost and improve the reconstruction efficiency. The method proposed in this paper gives a positive response to the possibility mentioned.

Optical microscopic imaging system has limited depth of focus (DOF). There is no exception for OSH physical system. Spatial resolution is also an important evaluation criterion for OSH image quality, but it is well known that the greater the DOF is, the lower the lateral resolution will be. Therefore, as the high lateral resolution remains unchanged, an expansion of the DOF is meaningful for OSH. In this paper, we analyze the maximum axial depth that can be recovered by l_2 norm and the proposed method.

The paper is organized as follows. Section 2 describes the two pupils OSH formulation and presents the proposed method. The proposed method is validated on both the whole and a half hologram data in section 3. A multi-planar experiment is conducted as well to further investigate the performance of the proposed method, followed by the analysis of the maximum axial depth. Finally, Section 4 gives conclusion about the OSH reconstruction method.

2. Theory and method

2.1. OSH formulation

Assuming the intensity of an object as $\varphi(x, y, z)$, the complex hologram obtained from OSH can be given by

#160246 - $15.00 USD Received 19 Dec 2011; revised 14 Feb 2012; accepted 20 Feb 2012; published 27 Feb 2012

$$g(x,y) = \int_{-\infty}^{+\infty} \varphi(x,y,z) * h(x,y;z)dz \approx \sum_{i=1}^{M} \varphi(x,y,z_i) * h(x,y;z_i), \quad (1)$$

where $h(x,y;z_i)$ is the point spread function of the OSH system, $\varphi(x,y,z_i)$ is the 2D sectional image, and asterisk denotes 2D spatial convolution involving the x and y coordinates. In the two-pupil OSH paradigm, $h(x,y;z_i)$ is given as

$$h(x,y;z_i) = -j\frac{1}{\lambda_0 z_i}\exp(j\frac{\pi}{\lambda_0 z_i}(x^2+y^2)), \quad (2)$$

where λ_0 is the wavelength of the laser used in the optical system. In optimization, it is necessary to describe Eq. (1) by matrix equation wherein the lexicographic ordering is employed. By lexicographic ordering, the $N \times N$ 2D hologram $g(x,y)$ converts into a vector G with the size of $N^2 \times 1$. Similarly, 2D sectional image $\varphi(x,y,z_i)$ becomes vector Φ_i with the size of $N^2 \times 1$, and the lexicographic ordering of $h(x,y;z_i)$ is presented by the matrix H_i with the size of $N^2 \times N^2$, such that $H_i\Phi_i$ equals $\varphi(x,y,z_i) * h(x,y;z_i)$ after lexicographic ordering. Considering noise ε, the equation for an object of M sectional images is presented as

$$G = \begin{bmatrix} H_1 H_2 \cdots H_M \end{bmatrix} \begin{bmatrix} \Phi_1 \\ \Phi_2 \\ \vdots \\ \Phi_M \end{bmatrix} + \varepsilon = H\Phi + \varepsilon, \quad (3)$$

where $H = \begin{bmatrix} H_1 H_2 \cdots H_M \end{bmatrix}$ and $\Phi = \begin{bmatrix} \Phi_1 \Phi_2 \cdots \Phi_M \end{bmatrix}^T$.

When dealing with the whole hologram data, we use $G = \begin{bmatrix} \mathrm{R(G)};I(\mathrm{G}) \end{bmatrix}$, $\varepsilon = \begin{bmatrix} \varepsilon_1;\varepsilon_2 \end{bmatrix}$ and $H_i = \begin{bmatrix} R(H_i);I(H_i) \end{bmatrix}$ ($i = 1,2\cdots,M$). The symbols $R(\cdot)$ and $I(\cdot)$ denote the real part and the imaginary part, respectively, of the quantity being bracketed. When using only the real part of the hologram, $G = \begin{bmatrix} \mathrm{R(G)} \end{bmatrix}$, $\varepsilon = \begin{bmatrix} \varepsilon_1 \end{bmatrix}$ and $H_i = \begin{bmatrix} R(H_i) \end{bmatrix}$ ($i = 1,2\cdots,M$) are used instead.

2.2. Computation simplification

Equation. (3) is the linear system of equations for OSH. By solving it, we can obtain all the sectional images simultaneously using optimization methods. Because of the large-scale data volume of the matrix H, optimization methods can only process relatively small data volume on limited memory desktop computer. For example, the original complex hologram data is 512×512 for one sectional image reconstruction. After lexicographic ordering, the size of matrix H is 262144×262144, beyond the capability of most ordinary desktop computers. Considering mainly involving multiplication of matrices, and multiplication of matrix and vector during optimization processing, two simplified computation modes are implemented to meet the large-scale data volume issue of OSH.

Mode 1: Matrix multiplication

To calculate the multiplication of two matrices, the following equation is required.

#160246 - $15.00 USD Received 19 Dec 2011; revised 14 Feb 2012; accepted 20 Feb 2012; published 27 Feb 2012

$$H^T H = \begin{bmatrix} H_1^T \\ H_2^T \\ \vdots \\ H_M^T \end{bmatrix} \begin{bmatrix} H_1 H_2 \cdots H_M \end{bmatrix} = \begin{bmatrix} H_1^T H_1 & H_1^T H_2 \cdots H_1^T H_M \\ H_2^T H_1 & H_2^T H_2 \cdots H_2^T H_M \\ \vdots & \\ H_M^T H_1 & H_M^T H_2 \cdots H_M^T H_M \end{bmatrix}, \quad (4)$$

where H_i has the property of block-circulant-circulant-block (BCCB) [20], corresponding to $h(x, y; z_i)$ after lexicographic ordering. While H_i^T is the transpose of H_i, it corresponds to $\tilde{h}(x, y; z_i)$ after lexicographic ordering.

The relationship between $\tilde{h}(x, y; z_i)$ and $h(x, y; z_i)$ is given by

$$\tilde{h}(x, y; z_i) = Rv(T(h(x, y; z_i))), \quad (5)$$

where the $T(\cdot)$ operator translates $h(x, y; z_i)$ towards negative x direction and y direction by 1 pixel; then the $Rv(\cdot)$ operator reverses it along the x axis and the y axis.

The calculation of the element in Eq. (4) requires the multiplication of matrices with size of $N^2 \times N^2$, which is hard to implement on limited memory desktop computer. In this paper, we use the convolution of matrices with size of $N \times N$ to replace the multiplication of matrices with size of $N^2 \times N^2$, as shown in Eq. (6) below. By using the Fast Fourier Transform (FFT) to calculate the matrix convolution, it also reduces the computation load significantly.

$$H_i^T H_j = lex(\tilde{h}(x, y; z_i) * h(x, y; z_j)), 1 \le i, j \le M, \quad (6)$$

where $lex(\cdot)$ denotes the lexicographic ordering operator. Based on Eq. (6), Eq. (4) can be processed block by block.

Mode 2: Matrix and vector multiplication

To calculate the multiplication of a matrix and a vector, the following equation is required.

$$HG = [H_1 H_2 \cdots H_M]G = \left[H_1 \mathrm{G}\, H_2 \mathrm{G} \cdots H_M G\right], \quad (7)$$

where H_i corresponds to $h(x, y; z_i)$ and G corresponds to $g(x, y)$ after lexicographic ordering.

Hence the multiplication of the matrix and the vector is shown as

$$H_i G = lex(h(x, y; z_i) * g(x, y)). \quad (8)$$

Similarly, Eq. (7) can be calculated block by block using Eq. (8).

2.3. Adaptively iterative shrinkage-thresholding (AIST) algorithm

The linear system of equations has been obtained in Eq. (3). If the error term ε is white noise whose energy is smaller than a given minimum δ, the ground truth sectional image can be well approximated by basis pursuit de-noising [21,22]:

$$\min \|\Phi\|_1, \textit{ subject to } \|G - H\Phi\|_2 \le \delta. \quad (9)$$

Using the Lagrangian method [23], the objective function of Eq. (9) can be rewritten as the unconstrained optimization equation:

$$\Phi^* = \arg\min_{\Phi} F(x) = \arg\min_{\Phi} \frac{1}{2}\|G - H\Phi\|_2 + \lambda \|\Phi\|_1, \quad (10)$$

#160246 - $15.00 USD Received 19 Dec 2011; revised 14 Feb 2012; accepted 20 Feb 2012; published 27 Feb 2012

where λ is the Lagrangian multiplier controlling the extent of sparsity. Under the separable property of the regularization term, the sparse reconstruction of the sectional image can be divided into some sub-problems, speeding the resolving of the original problem [24]. When the regularization is l_1 norm, a unique solution can be obtained.

In this paper, the adaptively iterative shrinkage-thresholding (AIST) algorithm is introduced to resolve the optimization equation of Eq. (10). The AIST method inherits the fast iterating of the iterative shrinkage-thresholding (IST) algorithm [25–27]. Different from the previous IST algorithm, the AIST algorithm adaptively converges to the global optimal solution using simplified computation. The adaptive methodology embodies in three aspects. First, an appropriate initial Lagrangian multiplier can be obtained by adaptively iterating of an exponential function, which is critical for the determination of the initial solution of Eq. (3). Second, after the acquired initial Lagrangian multiplier, a reasonable iterating Lagrangian multiplier sequence used for shrinkage soft-threshold is generated by another exponential function. Finally, multiple stopping criteria are employed, i.e., the relative error of the objective function, a priori knowledge of a terminating threshold (optional) and the maximum number of iteration.

Similar to IST, the AIST method first divides objective function into $f(\Phi)=\frac{1}{2}\left\|G-H\Phi\right\|_2^2$ and $g(\Phi)=\lambda\left\|\Phi\right\|_1$, where the second-order expansion of $f(\Phi)$ at Φ^k is given as

$$f(\Phi)\approx f(\Phi^k)+(\Phi-\Phi^k)^T\nabla f(\Phi^k)+\frac{1}{2}\left\|\Phi-\Phi^k\right\|_2^2\nabla^2 f(\Phi^k). \tag{11}$$

In practice, the Hessen matrix $\nabla^2 f(\Phi^k)$ can be approximated by a diagonal matrix $\alpha^k \mathrm{I}$, such that $\alpha^{k+1}(\Phi^{k+1}-\Phi^k)\approx\nabla f(\Phi^{k+1})-\nabla f(\Phi^k)$. As a result,

$$\alpha^{k+1}=\frac{(\Phi^{k+1}-\Phi^k)^T(\nabla f(\Phi^{k+1})-\nabla f(\Phi^k))}{(\Phi^{k+1}-\Phi^k)^T(\Phi^{k+1}-\Phi^k)}. \tag{12}$$

Hence, the update of Φ^k is,

$$\begin{aligned}\Phi^{k+1}&=\arg\min_{\Phi} f(x)+g(x)\\&\approx\arg\min_{\Phi}\left\{(\Phi-\Phi^k)^T\nabla f(\Phi^K)+\frac{\alpha^K}{2}\left\|\Phi-\Phi^k\right\|_2^2+\lambda^k\left\|\Phi\right\|_1\right\},\end{aligned} \tag{13}$$

where $\nabla f(\Phi^K)=H^T(H\Phi^K-G)$. According to Eq. (6) and Eq. (8), we rewrite $\nabla f(\Phi^K)$ as $\nabla f(\Phi^K)=H^T(H\Phi^K)-H^TG$, such that

$$\nabla f(\Phi^K)=\begin{bmatrix}\tilde{lex}(h_1*\gamma^k)\\ \tilde{lex}(h_2*\gamma^k)\\ \vdots\\ \tilde{lex}(h_M*\gamma^k)\end{bmatrix}-\begin{bmatrix}\tilde{lex}(h_1*g)\\ \tilde{lex}(h_2*g)\\ \vdots\\ \tilde{lex}(h_M*g)\end{bmatrix}, \tag{14}$$

where $\gamma^k=[lex(h_1*\varphi_1^k)+lex(h_2*\varphi_2^k)+\cdots+lex(h_M*\varphi_M^k)]$.

An equivalent update of Eq. (13) is that

$$\Phi^{k+1}=\arg\min_{\Phi}\frac{1}{2}\left\|\Phi-\theta\right\|_2+\frac{\lambda^k}{\alpha^k}\left\|\Phi\right\|_1, \tag{15}$$

#160246 - $15.00 USD Received 19 Dec 2011; revised 14 Feb 2012; accepted 20 Feb 2012; published 27 Feb 2012

where $\theta = \Phi^k - \frac{1}{\alpha^k}\nabla f(\Phi^k)$.

Using the equivalent soft-threshold, we obtain

$$\Phi^{k+1} = \arg\min_{\Phi} \frac{\left\|\Phi - \theta^k\right\|_2^2}{2} + \frac{\lambda\left\|\Phi\right\|_1}{\alpha^k} = soft(\theta^k, \frac{\lambda^k}{\alpha^k}) = \begin{cases} \operatorname{sgn}(\theta^k)\max\left\{\left|\theta\right|^{sep} - \frac{\lambda^k}{\alpha^k}, 0\right\}, & if\ \left|\theta\right|^{sep} > \frac{\lambda^k}{\alpha^k}, \\ 0, & otherwise, \end{cases} \tag{16}$$

where $\left|\theta\right|^{sep}$ represents that the absolute value is calculated separably, indicating that the implementation of soft-threshold is based on single element and integrates all the elements into a vector afterwards.

By now, only Lagrangian multiplier has not been determined. Because a reasonable Lagrangian multiplier is quite critical to the spares reconstruction of OSH, we have designed a dual factor exponential formulation:

$$\lambda^{k+1,p+1} = \lambda^{0,p}\exp(-\zeta_1 p - \zeta_2 k), k \geq 0, p \geq 0, \tag{17}$$

where an initial Lagrangian multiplier (at p level) is used for the determination of the sparsest initial solution and an iterating Lagrangian multiplier (at k level) is used for iterative shrinkage-thresholding.

In summary, **Algorithm 1** gives the pseudo-code of AIST algorithm to reconstruct the sectional image of OSH.

Algorithm 1 Implementation of adaptive iterative shrinkage-thresholding (AIST) algorithm

Requirement: matrix H, measured hologram vector G.

Initializing: Adaptive coefficient ζ_1 and ζ_2, $\lambda^{0,0}$, relative error coefficient $f(\varepsilon)$ and maximum iterating number *M*. $\Phi(p) = \vec{0}$, $p \leftarrow 0$.

1: **repeat**

2: $p \leftarrow p + 1$.

3: Shrinkage of the initial Lagrangian multiplier by $\lambda^{0,p} = \lambda^{0,p-1}\exp(-\zeta_1(p-1))$.

4: Update α^k according to Eq. (12).

5: Update solution $\Phi(p)$ using Eq. (16).

6: **until** $\Phi(p) \neq \vec{0}$.

7: Output initial Lagrangian multiplier $\lambda^{0,p}$ and re-initial $\Phi(k) = \Phi(p), k \leftarrow 0$.

8: **repeat**

9: $k \leftarrow k + 1$

10: Shrinkage of iterating Lagrangian multiplier by $\lambda^{k,p} = \lambda^{0,p-1}\exp(-\zeta_1(p-1) - \zeta_2(k-1))$.

11: **repeat**

12: Update α^k according to Eq. (12).

13: Update solution $\Phi(k)$ and objective function $F(\Phi(k))$ by Eq. (16) and Eq. (11) respectively.

14: **until** $F(\Phi(k)) < F(\Phi(k-1))$

15: **until** the stopping criteria are met.

#160246 - $15.00 USD Received 19 Dec 2011; revised 14 Feb 2012; accepted 20 Feb 2012; published 27 Feb 2012

3. Experiments and results

To validate the feasibility of the AIST method proposed in this paper, three verification experiments have been conducted. First, utilizing the hologram obtained by OSH physical system, the proposed method was verified on both the whole and a half hologram data. Second, the feasibility of the proposed method on multi-planar sectional image reconstruction has been investigated. Finally, the maximum axial depth which can be processed by OSH system has been studied at a given lateral resolution.

Subjective observation is not sufficient to demonstrate the performance of different methods. Herein a quantitative estimation named Image Quality (ImQ) [28] is adopted to compare the reconstruction performances, which is defined as

$$\mathrm{Im}\,Q = \frac{4\sigma_{\phi\hat{\phi}} E(\phi) E(\hat{\phi})}{(\sigma_{\phi}^2 + \sigma_{\hat{\phi}}^2)(E^2(\phi) + E^2(\hat{\phi}))}, \tag{18}$$

where ϕ is the original image and $\hat{\phi}$ is the estimated value of ϕ (i.e., the reconstructed image); $E(\phi)$ denotes the expectation of original image, while $E(\hat{\phi})$ denotes that of the reconstructed image; σ_{ϕ}^2 denotes the variance of original image and $\sigma_{\hat{\phi}}^2$ denotes that of the reconstructed image; and $\sigma_{\phi\hat{\phi}}$ denotes the mutual correlation of the original image and the reconstructed image.

3.1. Sectional image reconstruction by a half data

The optical part of OSH contains two pupils giving a spherical wave and a plane wave. The diameter of the plane wave is $25\,mm$, and the focal length of the lens used to give a spherical wave is $500\,mm$ [12]. Based on these two parameters, the calculated numerical aperture (NA) of the optical system used to record the complex hologram is 0.25. The excitation wavelength of the He-Ne laser is $632\,nm$. Two sectional images lie along the optical axis at $z_1 = 87\,cm$ and $z_2 = 107\,cm$. The real and imaginary parts of the complex hologram recorded by the physical OSH system are shown in Fig. 1, where the object consists of two transparencies with "S" located at z_1 and "H" at z_2.

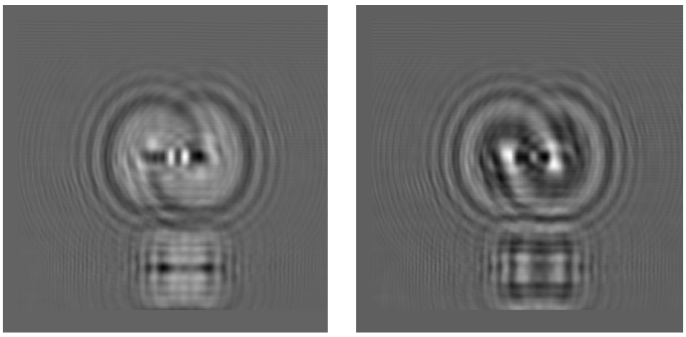

(a) (b)

Fig. 1. Complex hologram obtained by the physical OSH system. (a) Real part of the hologram. (b) Imaginary part of the hologram.

To verify the feasibility of the proposed method, we have conducted two experiments by the proposed method using both the whole hologram data and a half hologram data. For comparison sake, the conventional method and the l_2 norm method solved by conjugate gradient (CG) algorithm have been implemented as well.

#160246 - $15.00 USD Received 19 Dec 2011; revised 14 Feb 2012; accepted 20 Feb 2012; published 27 Feb 2012

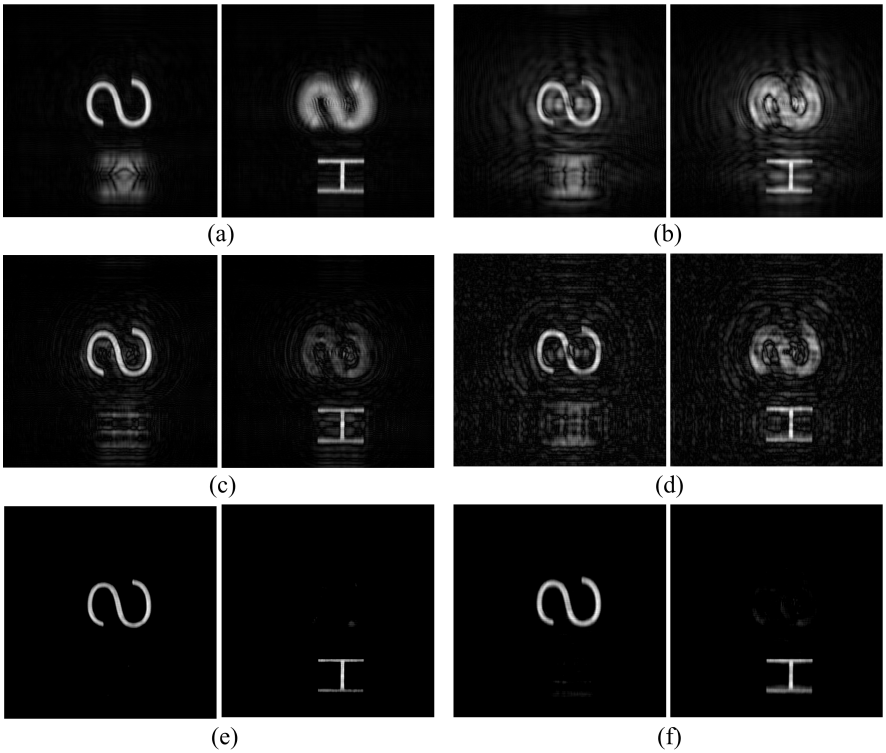

Fig. 2. Reconstruction results of OSH sectional images. (a) and (b) are results obtained by conventional method using the whole data and a half data. (c) and (d) are results obtained by l_2 norm method using the whole data and a half data. (e) and (f) are results obtained by the AIST method using the whole data and a half data.

"S" is the object of the first section, and "H" is that of the second section. The reconstructed results shown on the left two columns of Fig. 2 have been obtained using the whole hologram data. Compared with the results in Fig. 2(a), the blurred "H" in the first section and the blurred "S" in the second section becomes less striking in Fig. 2(c), which shows the advantage of the l_2 norm method to alleviate defocus noise over the conventional method. However, there are still some residual defocus noises in Fig. 2(c). Employing the AIST method, the desirable results have been obtained in Fig. 2(e). It is clear that the blurred noises in the reconstructed two sections disappear completely, thus demonstrating that the high performance of the proposed novel method on eliminating the out-of- focus haze.

The results on the right two columns have been obtained only using the real part of the complex hologram. The reconstructed sectional images in Fig. 2(d) deteriorate almost the same degree as those in Fig. 2(b). This is due to, in addition to the defocus noise, the twin image noise produced by the loss of the imaginary part of the complex hologram, which is hardly coped by the conventional method and the l_2 norm method. Nevertheless, the AIST method could solve this difficulty as shown in Fig. 2(f). The results are almost as good as those shown in Fig. 2(e). These results demonstrate the superiority of our proposed method on twin image noise reduction even though with a single channel of post-processing to obtain only a real hologram for reconstructions, thereby reducing the cost of the original OSH physical system.

3.2. Multi-planar object reconstruction

A multi-planar object simulation experiment has been implemented, where three sectional images (with different intensities) are located along the optical axis at $1.4\,mm$, $4.4\,mm$ and

#160246 - $15.00 USD Received 19 Dec 2011; revised 14 Feb 2012; accepted 20 Feb 2012; published 27 Feb 2012

7.4 mm . The lateral resolution is 1 μm . The real and imaginary parts of the complex hologram of the object are presented in Fig. 3.

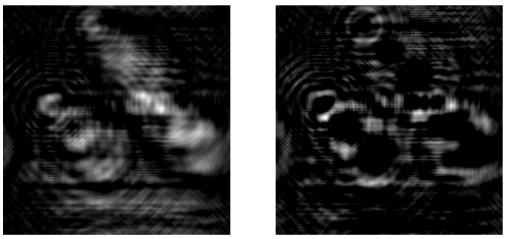

Fig. 3. Hologram of object with three planar sections. (a) Real part of the hologram. (b) Imaginary part of the hologram.

The reconstruction results of the l_2 norm method with the whole hologram are shown in Fig. 4(a). The results of the AIST method with the whole hologram and the half hologram are shown in Fig. 4(b) and 4(c), respectively. Both methods have the ability of reconstructing the in-focus object, but obviously the AIST method is superior in erasing the out-of-focus haze. Moreover, we have calculated the ImQs of Fig. 4(a), (b) and 4(c), and they are 0.4395, 0.9212 and 0.7779, respectively. These results further support the high performance of the proposed method on precise reconstruction.

In Fig. 4(b) and 4(c), we notice that the loss of the imaginary part of the hologram surely would decrease the reconstruction quality but the results are acceptable. The results of the l_2 norm method with a half hologram, however, degenerate seriously.

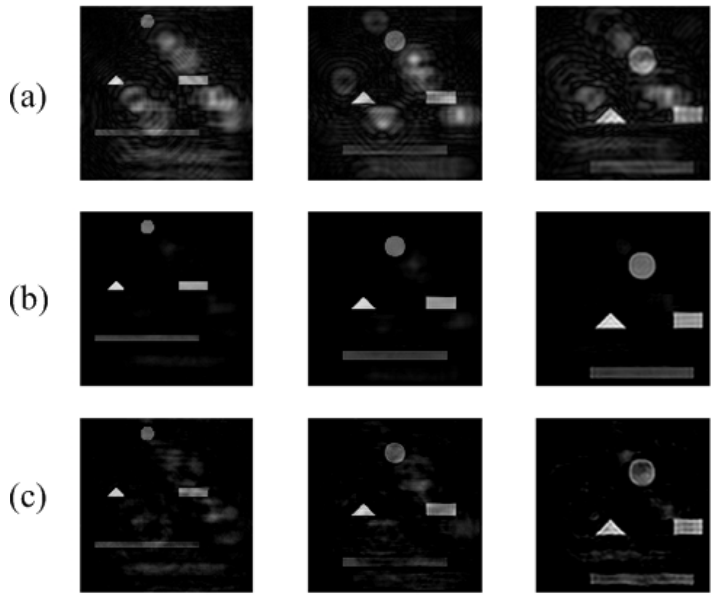

Fig. 4. Reconstruction results of the l_2 norm method and the AIST method. (a) Results of l_2 norm method with the whole hologram. (b) Results of the AIST method with the whole hologram. (c) Results of the AIST method with the real part of the hologram.

3.3. DOF analysis

For 3D imaging, there is a compromise between the lateral resolution and the depth of focus (DOF). Herein we analyze the maximum DOF of the l_2 norm and the proposed AIST method.

#160246 - $15.00 USD Received 19 Dec 2011; revised 14 Feb 2012; accepted 20 Feb 2012; published 27 Feb 2012

We employed two sectional images as shown in Fig. 5. Different from previous experiments, we fix the location of one section at the depth of 1.0 *mm* but vary the separation of the second section to the first section from 0.2 *mm* to 49.5 *mm* . The system has 1 μm lateral resolution.

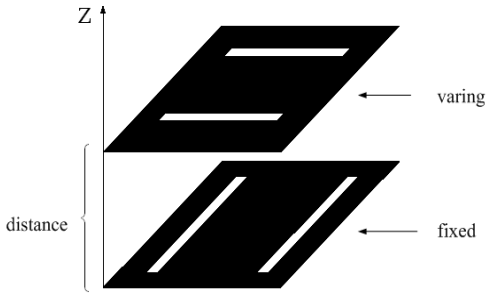

Fig. 5. Sectional images illustration. The first sectional image is fixed at the depth of 1.0mm, while the second sectional image varies from0.2mm to 49.5mm.

Figure 6 gives the reconstruction results of the two methods and Table 1 shows the corresponding ImQs. When the distance of two sections is 0.2 *mm* , the AIST method obtains a considerably good reconstruction, but the l_2 norm method cannot distinguish the two sections. The highest ImQ (0.9780) of the AIST method is acquired when the distance is 1 *mm* between the two sections, as shown in Fig. 6(d). But the corresponding ImQ of the l_2 norm is only 0.6852(Fig. 6(c)). When the distance is 9 *mm* , the l_2 norm method arrives its maximum at 0.7277 (Fig. 6(e)), however, the ImQ of the AIST method is as high as 0.9210 (Fig. 6(f)). Moreover, when the distance of two sections is 49.5 *mm* apart from each others, the ImQ of the AIST method and the l_2 norm method is 0.8085 and 0.4905, respectively. The latter method has completely loss the capability to reconstruct the second sectional image (Fig. 6(g)).

Table 1. ImQ's of the Reconstruction Results

Distance Separation	*0.2mm*	*1.0mm*	*9.0mm*	*49.5mm*
AIST	0.9083	0.9780	0.9210	0.8085
l_2 norm	0.6650	0.6852	0.7277	0.4905

The ImQ curves of the AIST method and the l_2 norm method from 0.2 *mm* to 49.5 *mm* are shown in Fig. 7. The performance of the conventional method is worse than the l_2 norm method, hence its result is not presented. Although there are some disturbances, the AIST method keeps high ImQs at all the distance points as compared with the l_2 norm method. Moreover, the ImQ of the AIST method descends slowly, while it is not the case for the l_2 norm method. The result implies that the proposed method is non-sensitive to the distance increase between two sections.

From the results indicated, the proposed AIST method may provide a solution to expand the maximum recoverable depth.

#160246 - $15.00 USD Received 19 Dec 2011; revised 14 Feb 2012; accepted 20 Feb 2012; published 27 Feb 2012

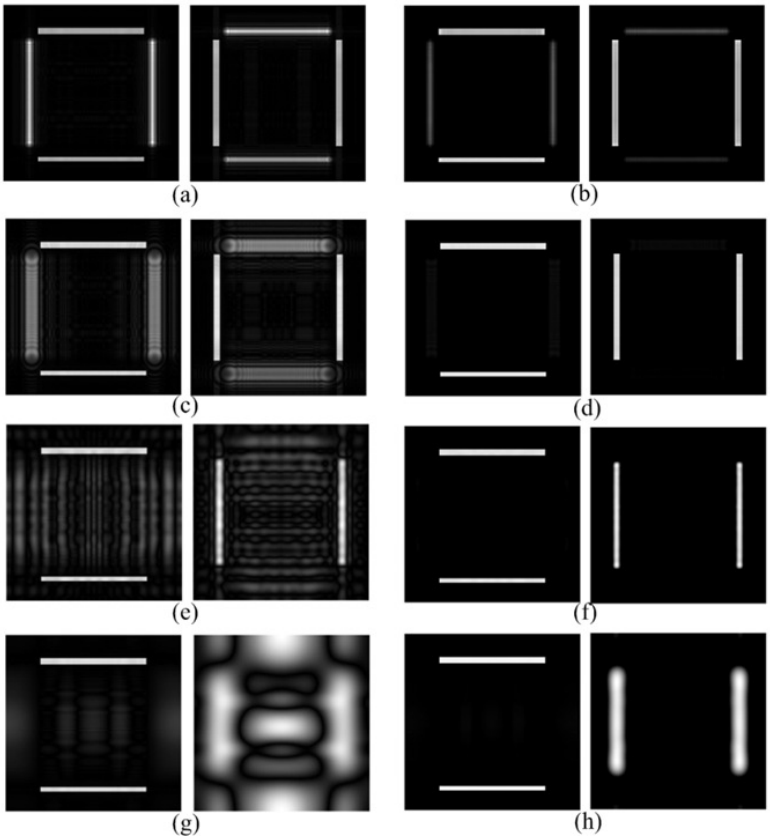

Fig. 6. Reconstruction results by the the l_2 norm method and the AIST method. The left two columns are the results of the l_2 norm method, and the right two columns are the results of the AIST method. The distance between two sectional images is (a) (b) 0.2 *mm* , (c) (d) 1.0 *mm* , (e) (f) 9.0 *mm* , and (g) (h) 49.5 *mm* respectively.

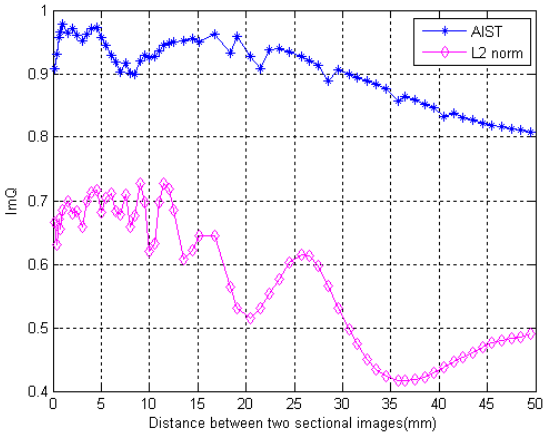

Fig. 7. ImQ of the AIST method and the l_2 norm method.

#160246 - $15.00 USD Received 19 Dec 2011; revised 14 Feb 2012; accepted 20 Feb 2012; published 27 Feb 2012

4. Conclusion

We have proposed an AIST method for sectional image reconstruction in OSH. The reconstruction results have been improved significantly as compared with the conventional method and the l_2 norm method. More importantly the twin image noise has been eliminated using only a half of the original hologram data (i.e., keeping the real part of the complex hologram), while both the real and the imaginary parts of the hologram data are needed for the conventional and the l_2 norm method. We also have applied the proposed method to a multi-planar object to investigate its validity on a relatively complex situation. Finally we have analyzed the maximum reconstructed depth at 1 μm lateral resolution, and the results demonstrated that the AIST method has the ability to extend the maximum reconstruction depth. This study has contributed to the increase of the imaging depth in OSH with relatively high resolution, and will widen its prospect on the imaging of thick specimens.

Acknowledgments

This work is supported by the Program of the National Basic Research and Development Program of China (973) under Grant No. 2011CB707702, the National Natural Science Foundation of China under Grant Nos. 81090272, 81101083, 81101084, 81101100, 81000632, 30900334, the Shaanxi Provincial Natural Science Foundation Research Project under Grant No. 2009JQ8018, the Fundamental Research Funds for the Central Universities, and Basic Science Research Program through the National Research Foundation of Korea (NRF) funded by the Ministry of Education, Science and Technology (NRF-2009-0087476).

#160246 - $15.00 USD Received 19 Dec 2011; revised 14 Feb 2012; accepted 20 Feb 2012; published 27 Feb 2012